Emergent Quasicrystalline Symmetry in Light-Induced Quantum Phase Transitions

Farokh Mivehvar,[1,*] Helmut Ritsch,[1] and Francesco Piazza[2]
[1]Institut für Theoretische Physik, Universität Innsbruck, A-6020 Innsbruck, Austria
[2]Max-Planck-Institut für Physik komplexer Systeme, D-01187 Dresden, Germany

(Received 5 August 2019; revised manuscript received 24 October 2019; published 22 November 2019)

The discovery of quasicrystals with crystallographically forbidden rotational symmetries has changed the notion of the ordering in materials, yet little is known about the dynamical emergence of such exotic forms of order. Here we theoretically study a nonequilibrium cavity-QED setup realizing a zero-temperature quantum phase transition from a homogeneous Bose-Einstein condensate to a quasicrystalline phase via collective superradiant light scattering. Across the superradiant phase transition, collective light scattering creates a dynamical, quasicrystalline optical potential for the atoms. Remarkably, the quasicrystalline potential is "emergent" as its eightfold rotational symmetry is not present in the Hamiltonian of the system, rather appears solely in the low-energy states. For sufficiently strong two-body contact interactions between atoms, a quasicrystalline order is stabilized in the system, while for weakly interacting atoms the condensate is localized in one or few of the deepest minima of the quasicrystalline potential.

DOI: 10.1103/PhysRevLett.123.210604

Introduction.—Quasicrystals are quasiordered (or orientationally ordered) materials with no exact translational symmetry, rather with crystallographically forbidden rotational symmetries [1]. They possess rotational symmetries, such as five-, seven-, eightfold rotational symmetries, as discovered from their diffraction patterns first by Shechtman *et al.* in 1984 [2]. Therefore, they are not periodic and do not belong to any of the crystallographic space groups. Interestingly, quasicrystals, related to aperiodic tilings, can be considered as projections of higher dimensional periodic lattices [3–5]. Despite extensive theoretical and experimental research since their discovery [6], there are still many fundamental open questions concerning the formation and nature of quasicrystals. For instance, it is still not completely clear whether quasicrystals are only entropy-stabilized high-temperature states or can also be thermodynamically stable at low temperatures [7]. In particular, the conditions and nature of quasicrystal growth are under debate with a lack of a generally accepted model.

Ultracold atoms trapped in laser-created tailored optical potentials have proven to be a versatile platform for simulating and exploring exotic solid-state models in a controllable manner [8]. In this context, the recent loading of a Bose-Einstein condensate (BEC) into a specially designed quasicrystal optical potential led to the observation of a diffraction pattern with a forbidden eightfold rotational symmetry and has opened a new perspective on studying quasicrystals [9]. This now allows for a detailed experimental investigation of the nature of quasicrystals and other theoretically predicted phenomena such as the interplay between quasiordering and localization [10–16]. Unlike natural quasicrystals, however, the quasicrystallization in these systems is *not* dynamically emergent and spontaneous [17,18], rather induced by the underlying optical potentials imposed on the atoms by prescribed external lasers. Recently, a few schemes based on spin-orbit-coupled BECs were proposed to realize quantum phase transitions to quasicrystals [19,20], where quasicrystalline rotational symmetries appear in these systems due to the interplay between the spin-orbit coupling and two-body interactions—i.e., two competing length scales. This competition [21–28] has been identified to be also the relevant mechanism for the quasicrystallization in soft matter [29–33].

In this Letter we propose an alternative, novel scenario for the spontaneous formation of a quasicrystal based on a dynamical optical potential for ultracold atoms inside an optical cavity setup [34–56], where a quasicrystalline symmetry *emerges* in the low-energy sector across a superradiant phase transition. The setup consists of four identical linear cavities arranged in a plane with a common center such that they make a 45° angle with one another. A Bose gas is tightly confined in the direction perpendicular to the plane at the intersection of these initially empty four cavities, and is strongly coupled to a single mode of each cavity. The BEC is also driven by a spatially uniform pump laser propagating perpendicular to the cavity-BEC plane as depicted in Fig. 1.

At low pump-laser strengths, the system is in the normal homogenous (NH) state, where the condensate is uniform and the photon scattering from the pump into the cavities is strongly suppressed. Beyond a critical laser strength, atoms collectively scatter photons from the pump into the cavities

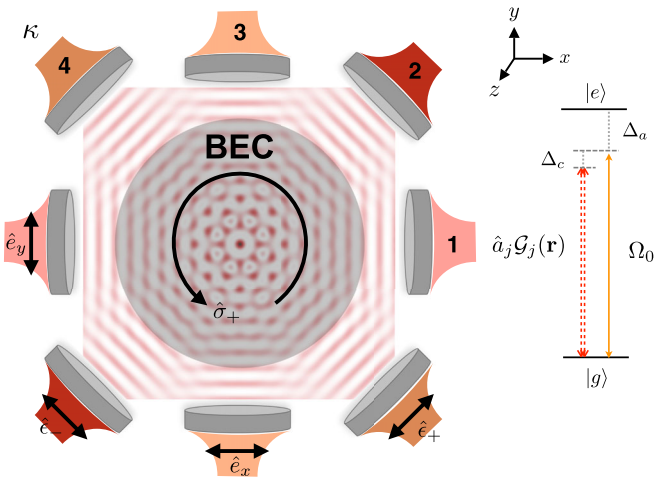

FIG. 1. Schematic view of a quasi-two-dimensional driven BEC inside four identical crossed linear cavities, which make a 45° angle with one another. The driving laser with the right circular polarization $\hat{\sigma}_+$ propagates along the z direction and it is not shown explicitly in the figure. The inset depicts the internal atom-photon couplings.

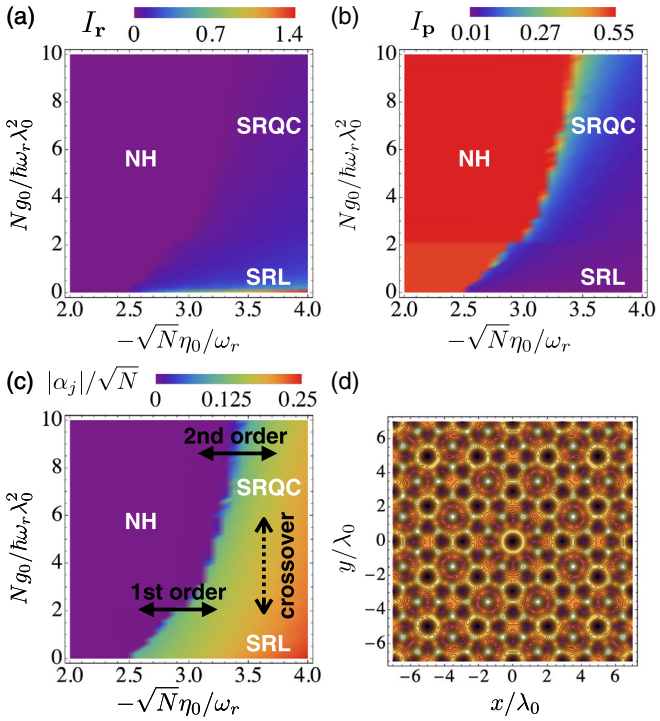

FIG. 2. The phase diagram of the system in the $\{Ng_0/\hbar\omega_r\lambda_0^2, \sqrt{N}\eta_0/\omega_r\}$ parameter plane. The system exhibits three distinct phases: normal homogenous, superradiant localized, and superradiant quasicrystal states. The inverse participation ratios $\{I_{\mathbf{r}}, I_{\mathbf{p}}\}$ as well as the field amplitudes $|\alpha_j|$ display nonanalytical behavior on the onset of the superradiant phase transition as shown in (a)–(c). The order and the nature of the transitions are indicated in (c). A typical emergent superradiant quasicrystalline optical potential with the eightfold rotational symmetry C_8 located at the origin is presented in (d). The parameters are set to $(\Delta_c, \kappa, N\mathcal{G}_0^2/\Delta_a) = (-10, 10, -1)\omega_r$.

as atomic density fluctuations are amplified due to the field backaction. Consequently, the pump and built-up cavity fields interfere, leading to the formation of a nonperiodic, dynamic superradiant quasicrystalline potential for the atoms, which possesses an *emergent* eightfold rotational symmetry C_8; see Figs. 2(c) and 2(d). Although the Hamiltonian of the system does not possess this eightfold rotational symmetry, across the superradiant phase transition this symmetry emerges in the low-lying energy sector thanks to specific cavity-field *amplitudes* and *phases* chosen spontaneously by the system. The center of the quasicrystal (i.e., the location of the C_8 rotational axis) is fixed via a process of spontaneous breaking of four approximate discrete $\mathbf{Z}_2$ symmetries. The mechanism of emerging global C_8 symmetry here is reminiscent of emergent global [57–64] and local gauge [65–69] symmetries found in some other models in the proximity of certain quantum phase transitions and/or in some quantum phases.

In the superradiant phase, the atoms in turn self-order in this emergent quasicrystalline potential. For sufficiently strong two-body repulsive contact interactions between the atoms, a superradiant quasicrystalline (SRQC) order is stabilized in the system, where momentum components of the self-ordered BEC wave function exhibit an eightfold rotational symmetry as shown in Fig. 3(b). On the contrary, for weakly interacting atoms the condensate is localized in one or few of the deepest minima of the quasicrystalline potential. Correspondingly, the many occupied momentum components of the condensate wave function show a Gaussian distribution. We thus refer to this state as the superradiant localized (SRL) phase.

Model.—Consider ultracold bosonic atoms trapped in a quasi-two-dimensional "circular" box potential $V_{\text{box}}(\mathbf{r})$ in the x-y plane and off-resonantly driven in the z direction by a right circularly polarized $\hat{\sigma}_+$ pump laser with Rabi frequency $\Omega_0 \propto \langle e|\sigma_+ \cdot \mathbf{d}|g\rangle$ and wave number $k_0 = 2\pi/\lambda_0$. The atomic internal states $\{|g\rangle, |e\rangle\}$ satisfy the selection rule $m_e - m_g = 1$. Furthermore, the atomic transition $|g\rangle \leftrightarrow |e\rangle$ is also off-resonantly coupled to four initially empty, in-plane polarized, quantized electromagnetic modes, each belonging to one linear cavity. The atom-cavity couplings are given by $\mathcal{G}_j(\mathbf{r}) = e^{i\theta_j}\mathcal{G}_{0j}\cos(\mathbf{k}_j \cdot \mathbf{r})$, where $\mathbf{k}_1 = k_0\hat{e}_x$, $\mathbf{k}_3 = k_0\hat{e}_y$, and $\mathbf{k}_{2,4} = k_0(\hat{e}_x \pm \hat{e}_y)/\sqrt{2}$, and $\mathcal{G}_{0j}$ are the maximum atom-cavity couplings per photon. Here, $\hat{e}_x$ ($\hat{e}_y$) is the unit vector along the x (y) direction and $i^2 = -1$. The wave number of the cavity modes have been assumed to be equal to the wave number of the laser, $|\mathbf{k}_j| = k_0$, as the cavity frequencies $\omega_c \equiv \omega_{c1} = \cdots = \omega_{c4}$ are taken to be close to resonant with laser frequency $\omega_0 = ck_0$. The phase factors $\theta_1 = \pi/2$, $\theta_2 = 5\pi/4$, $\theta_3 = \pi$, and $\theta_4 = 3\pi/4$ arise due to the

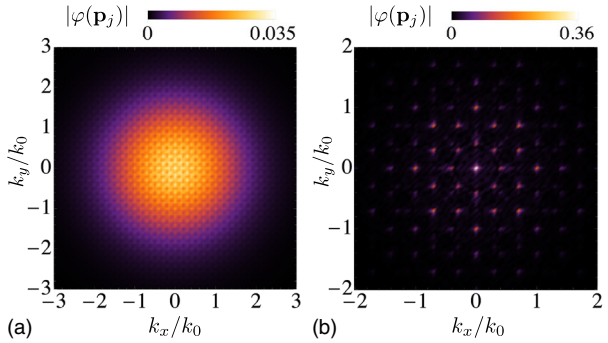

FIG. 3. Typical atomic momentum distribution in the SRL (a) and SRQC (b) phases. The momentum distribution in the SRQC state exhibits a clear eightfold rotational symmetry, with occupied fractional momentum states. In the SRL phase, it is, however, a Gaussian with remnants of the eightfold rotational symmetry on top of it. The parameters are set to $\sqrt{N}\eta_0/\omega_r = 4$ and $Ng_0/\hbar\omega_r\lambda_0^2 = 0$ (a) and 5 (b), with the rest being the same as Fig. 2.

projection of the in-plane linear polarizations $\hat{e}_{x,y}$ and $\hat{e}_\pm = (\hat{e}_x \pm \hat{e}_y)/\sqrt{2}$ of the cavity fields onto the right circular polarization $\hat{\sigma}_+$ as detailed in the Supplemental Material [70]. The system is depicted schematically in Fig. 1.

Assuming that the atomic detuning $\Delta_a \equiv \omega_0 - \omega_a < 0$, with ω_a being the atomic transition frequency between the ground state $|g\rangle$ and the electronic excited state $|e\rangle$, is very large, the atomic excited state can be adiabatically eliminated. This yields an effective Hamiltonian $\hat{H}_{\rm eff} = \int \hat{\psi}^\dagger(\mathbf{r})\hat{\mathcal{H}}_{0,\rm eff}\hat{\psi}(\mathbf{r})d\mathbf{r} + \hat{H}_{\rm int} - \hbar\Delta_c \sum_j \hat{a}_j^\dagger \hat{a}_j$ for the system, with the effective single-particle Hamiltonian density in the rotating-frame of the laser,

$$\hat{\mathcal{H}}_{0,\rm eff} = -\frac{\hbar^2}{2M}\nabla^2 + V_{\rm box}(\mathbf{r}) + \frac{\hbar}{\Delta_a}\left|\Omega_0 + \sum_{j=1}^{4}\hat{a}_j\mathcal{G}_j(\mathbf{r})\right|^2, \quad (1)$$

and the two-body interaction Hamiltonian,

$$\hat{H}_{\rm int} = g_0 \int \hat{\psi}^\dagger(\mathbf{r})\hat{\psi}^\dagger(\mathbf{r})\hat{\psi}(\mathbf{r})\hat{\psi}(\mathbf{r})d\mathbf{r}. \quad (2)$$

Here $\hat{\psi}(\mathbf{r})$ and $\hat{a}_j$ are the atomic and photonic bosonic field operators, respectively, $\Delta_c \equiv \omega_0 - \omega_c$ is the cavity detunings with respect to the laser, and g_0 is the strength of the two-body contact interactions proportional to the s-wave scattering length.

Mean-field approach.—We consider the thermodynamic limit, where the quantum fluctuations are negligible in two dimensions and the mean-field approach is justified [71]: $\hat{\psi} \to \psi \equiv \langle\hat{\psi}\rangle$ and $\hat{a}_j \to \alpha_j = |\alpha_j|e^{i\gamma_j} \equiv \langle\hat{a}_j\rangle$. Hence we solve the mean-field Gross-Pitaevskii equation

$$(\langle\hat{\mathcal{H}}_{0,\rm eff}\rangle + g_0 n(\mathbf{r}))\psi(\mathbf{r}) = \mu\psi(\mathbf{r}), \quad (3)$$

along with the self-consistent solution of the steady-state cavity-field amplitudes $i\hbar\langle\partial_t\hat{a}_j\rangle = \langle[\hat{a}_j, \hat{H}_{\rm eff}]\rangle - i\hbar\kappa\langle\hat{a}_j\rangle = 0$,

$$-\delta_{cj}\alpha_j + \sum_{\ell\neq j} c_{j\ell}\alpha_\ell + \eta_j = 0; \qquad j,\ell = 1,2,3,4. \quad (4)$$

Here, $\langle\hat{\mathcal{H}}_{0,\rm eff}\rangle$ is the mean-field single-particle Hamiltonian density corresponding to Eq. (1) with $\hat{a}_j \to \alpha_j$, $n(\mathbf{r}) = |\psi(\mathbf{r})|^2$ is the local atomic density, μ is the chemical potential, κ is the decay rate of the cavity fields due to photon losses through the cavity mirrors, and we have introduced the following symbols for the shorthand:

$$\begin{aligned}\delta_{cj} &= \Delta_c + i\kappa - \frac{1}{\Delta_a}\int |\mathcal{G}_j(\mathbf{r})|^2 n(\mathbf{r})d\mathbf{r},\\ c_{j\ell} &= \frac{1}{\Delta_a}\int \mathcal{G}_j^*(\mathbf{r})\mathcal{G}_\ell(\mathbf{r})n(\mathbf{r})d\mathbf{r},\\ \eta_j &= \frac{\Omega_0}{\Delta_a}\int \mathcal{G}_j^*(\mathbf{r})n(\mathbf{r})d\mathbf{r}.\end{aligned} \quad (5)$$

This approach neglects the heating induced by cavity losses, which is well justified as the corresponding rate is suppressed with the inverse system's size [72]. Without loss of generality and for the sake of simplicity, in the following we set $\mathcal{G}_{0j}$ and Ω_0 to be real and only focus on the most interesting case of symmetric coupling to all cavities, $\mathcal{G}_0 \equiv \mathcal{G}_{01} = \cdots = \mathcal{G}_{04}$.

Since the system is not translationally invariant, we solve Eqs. (3) and (4) in a square box of size $L_x \times L_y = L^2 = 20\lambda_0 \times 20\lambda_0$ centered at the origin $\mathbf{r} = 0$ with open boundary conditions and a circular box potential of the form $V_{\rm box}(\mathbf{r}) = 0$ for $|\mathbf{r}| < L/2$, otherwise, $V_{\rm box}(\mathbf{r}) \to \infty$ [73]. In order to characterize the BEC density and momentum distributions, we exploit the inverse participation ratios [74,75],

$$I_{\mathbf{r}} = \int |\psi(\mathbf{r})|^4 d\mathbf{r} \Big/ \left(\int |\psi(\mathbf{r})|^2 d\mathbf{r}\right)^2, \quad (6a)$$

$$I_{\mathbf{p}} = \sum_{\mathbf{p}_j} |\varphi(\mathbf{p}_j)|^4 / (\sum_{\mathbf{p}_j} |\varphi(\mathbf{p}_j)|^2)^2, \quad (6b)$$

where $\varphi(\mathbf{p}) = \int e^{i\mathbf{p}\cdot\mathbf{r}}\psi(\mathbf{r})d\mathbf{r}/L^2$ is the Fourier transform of the condensate wave function $\psi(\mathbf{r})$. $I_{\mathbf{r}}$ and $I_{\mathbf{p}}$ quantify how localized the atomic distributions are in position and momentum spaces, respectively. For instance, for a uniform density distribution $I_{\mathbf{r}}$ approaches zero in the thermodynamic limit as $1/L^2$, while $I_{\mathbf{p}}$ approaches 1.

Phase diagram and emergent symmetries.—Figure 2 shows the phase diagram of the system in the $\{Ng_0/\hbar\omega_r\lambda_0^2, \sqrt{N}\eta_0/\omega_r\}$ parameter plane, where N is the number of the atoms, $\omega_r \equiv \hbar k_0^2/2M$ is the recoil frequency, and $\eta_0 \equiv \mathcal{G}_0\Omega_0/\Delta_a$ is the effective pump strength [76]. The inverse participation ratios in position

$I_{\mathbf{r}}$ and momentum $I_{\mathbf{p}}$ space are illustrated in Figs. 2(a) and 2(b), respectively. The corresponding rescaled steady-state field amplitudes $|\alpha_j|/\sqrt{N}$ are presented in Fig. 2(c).

Below the laser-strength threshold $\eta_0^c(g_0)$ the system is in the NH state, where there is no photon in any of the cavities and the atoms are uniformly (saving for the boundary) distributed over the box potential V_{box}. Therefore, the position-space (momentum-space) participation ratio $I_{\mathbf{r}}$ ($I_{\mathbf{p}}$) assumes its smallest (largest) value in this phase.

By increasing the pump-laser strength η_0 above the threshold $\eta_0^c(g_0)$, the uniform atomic distribution starts to become unstable. Fluctuations in the atomic density result in constructive photon scattering from the pump laser into the cavity modes. The interference of the pump and built-up cavity fields creates an emergent optical potential, favoring density modulations which in turn further enhance collective photon scattering into the cavity modes. This starts a runaway process towards a superradiant phase where $|\alpha_j| > 0$ for all j. Both participation ratios change at the onset of the superradiant phase transition. In particular, the momentum-space participation ratio $I_{\mathbf{p}}$ displays a sharp drop, signaling the occupation of many momentum states. In the superradiant phase $\alpha_j = |\alpha_j| e^{i\gamma_j} \neq 0$, not only are the absolute values of all the field amplitudes equal $|\alpha| \equiv |\alpha_1| = \cdots = |\alpha_4| \neq 0$, but also the phase of each field amplitude is locked at $\gamma_j = \gamma_0 - \theta_j$ or $\gamma_0 + \pi - \theta_j$, where γ_0 is a common phase introduced due to the nonzero cavity-field decay rate $\kappa \neq 0$.

The single-particle Hamiltonian density $\hat{\mathcal{H}}_{0,\text{eff}}$, Eq. (1), possesses a symmetry which we denote by $\tilde{C}_8$: an eightfold rotation C_8 around the z axis with the transformation $x \to x' = (x+y)/\sqrt{2}$ and $y \to y' = (y-x)/\sqrt{2}$ followed by the field transformation $\hat{a}_1 \to \hat{a}_2 e^{-i(\theta_1-\theta_2)}$, $\hat{a}_2 \to \hat{a}_3 e^{-i(\theta_2-\theta_3)}$, $\hat{a}_3 \to \hat{a}_4 e^{-i(\theta_3-\theta_4)}$, and $\hat{a}_4 \to \hat{a}_1 e^{-i(\theta_4-\theta_1)}$. Note that $\hat{\mathcal{H}}_{0,\text{eff}}$ is *not* invariant under the sole action of the C_8 rotation. Nonetheless, an eightfold rotational symmetry C_8 *emerges* in the low-energy sector of the superradiant phase due to the above-mentioned amplitude and phase locking of the cavity fields: $|\alpha| \equiv |\alpha_1| = \cdots = |\alpha_4| \neq 0$, and $\gamma_j + \theta_j = 0$ or π (γ_0 is an immaterial overall common phase shift discarded here for the sake of simplicity); see Supplemental Material for more details [70]. The two possible choices of phase, $-\theta_j$ or $\pi - \theta_j$, for each field amplitude correspond to a $\mathbf{Z}_2$ symmetry for each cavity. The phases γ_j of the field amplitudes determine the center of the quasicrystal (i.e., the location of the C_8 rotational axis). Figure 2(d) shows an example for the case $\gamma_j = -\theta_j$ for $j = 1, \ldots, 4$. Therefore, at the onset of the superradiant phase transition, the center of the emergent quasicrystal is fixed through the spontaneous breaking of an approximate $\otimes_{j=1}^{4}\, \mathbf{Z}_2$ symmetry as explained in detail in the following.

For the case $\gamma_j = -\theta_j$ ($\gamma_j = \pi - \theta_j$) for all the modes $j = 1, \ldots, 4$, all fields have positive (negative) antinode at the origin $\mathbf{r} = 0$. Therefore, the C_8 rotational axis is located at the origin, defining the center of the quasicrystal. Whereas, e.g., for the case that $\gamma_1 = \pi - \theta_1$ and $\gamma_j = -\theta_j$ for the rest (i.e., $j = 2, 3, 4$), the rotational axis is shifted along the x axis and its location x_o has to satisfy both $x_o = (m + 1/2)\lambda_0$ and $x_o = \sqrt{2} l \lambda_0$, with m and l being two integers. However, these two conditions are not exactly consistent with each other for any two finite integers m and l, as the first equation yields a rational number while the second one an irrational number. One might, therefore, claim that the two conditions may coincide at infinity, implying that the center of the quasicrystal is located at $x_o \to \pm\infty$.

The self-ordered condensate density in the superradiant phase depends on the interplay between the emergent quasicrystal optical potential and the two-body repulsive contact interaction g_0. Since the optical potential is not periodic, it can act as a disordered potential for the BEC, favoring Anderson-type localization [77,78]. On the other hand, this is counteracted by the two-body repulsive interactions. This competition determines the self-ordered BEC density.

In the weakly interacting regime, the quasicrystal potential dominates over the two-body interactions and the condensate localizes in one or few of deepest minima of the quasicrystal potential. In this localized phase the atoms scatter more photons from the pump laser into the cavity modes due to constructive interference: the more atoms are condensed in the same potential minimum, the more photons are scattered with the same phase. This SRL regime is the lower right corner in Figs. 2(a)–2(c). The inverse participation ratio in the position space $I_{\mathbf{r}}$ attains its largest values in this phase. A typical momentum distribution of the self-ordered SRL state is shown in Fig. 3(a); strong localization here leads to a Gaussian momentum distribution with remnants of the underlying eightfold rotational symmetry superimposed on it.

In the strongly interacting regime on the other hand, it is energetically more favorable for the atoms to occupy different global and local minima of the quasicrystal optical potential. For sufficiently strong two-body contact interactions, a quasicrystalline density order is stabilized in the system as apparent from the momentum distribution of self-ordered states, shown in Fig. 3(b) for a typical state in this regime. Note the fractal distribution, a characteristic of quasicrystalline order indicating that the two-dimensional momentum space cannot be spanned by only two reciprocal primitive vectors. Here the two-dimensional momentum space is spanned by four incommensurate cavity wave vectors $\{\mathbf{k}_1, \ldots, \mathbf{k}_4\}$, resulting in dense and self-similar momentum diffraction peaks [9]. Furthermore, regardless of the center of the quasicrystal, all the sixteen $\otimes_{j=1}^{4}\, \mathbf{Z}_2$ symmetry-broken states exhibit an identical momentum

distribution, saving for small finite-size effects [70]. Therefore, we refer to this phase as the SRQC state.

One can identify the field amplitude $|\alpha|$ (recall that $|\alpha| \equiv |\alpha_1| = \cdots = |\alpha_4|$) as an order parameter. It is zero in the NH phase and acquires nonzero values in the SRL and SRQC phases. The order parameter $|\alpha|$ exhibits a discontinuous jump in the transition from the NH phase to the SRL state, signaling a first order phase transition. The transition from the NH state to the SRQC phase is also first order in the weakly interacting regime, but becomes second order in the strongly interacting regime. On the other hand, we have only a crossover between the SRL and SRQC phases, as the order parameter $|\alpha|$ changes smoothly in the transition. For clarity, various cuts from the phase diagrams are presented in the Supplemental Material for different transitions [70].

Conclusions.—We proposed and studied a novel cavity-QED setup where a quantum phase transition from a uniform BEC to a quasicrystalline state with an emergent eightfold rotational symmetry can be realized and monitored nondestructively via the amplitudes $|\alpha_1| = \cdots = |\alpha_4| \neq 0$ and phases $\gamma_j = \gamma_0 - \theta_j$ or $\gamma_0 + \pi - \theta_j$ of the cavity-output fields. The proposed setup is a realistic generalization of the state of the art in the experiment, namely, the two-crossed cavity setup [39–41] and the bow-tie cavities [46]. Analogous setups can allow the study of quasicrystals with other emergent rotational symmetries such as five- and sevenfold rotational symmetries. Our proposed model differs from all previously proposed schemes including those based on spin-orbit coupling [19,20]: in the previous proposals the quasicrystalline states have a *broken* symmetry with respect to corresponding single-particle Hamiltonians while here the superradiant quasicrystalline state has an *emergent* symmetry. Furthermore, the quantum phase transition to the quasicrystalline and localized states can be attributed to the interplay between two-body contact interaction and cavity-mediated long-range interactions. Therefore, our work demonstrates that cavity QED offers a novel nondemolishing platform [79–82] for exploring the spontaneous formation and stabilization mechanisms of a quasicrystal at very low temperatures. It opens a new avenue for realizing in state-of-the-art quantum-gas–cavity systems quantum phase transitions which are accompanied by an emergent (C_8 rotational) symmetry. Our considered system may also support exotic vestigial orders in some parameter regimes [83].

We acknowledge inspiring discussions with Julian Léonard. F. M. is grateful to Stefan Ostermann for fruitful discussions regarding numerics. F. M. is supported by the Lise-Meitner Fellowship M2438-NBL of the Austrian Science Fund (FWF), and the International Joint Project No. I3964-N27 of the FWF and the National Agency for Research (ANR) of France.

*Corresponding author.
farokh.mivehvar@uibk.ac.at

[1] D. Levine and P. J. Steinhardt, Quasicrystals: A New Class of Ordered Structures, Phys. Rev. Lett. **53**, 2477 (1984).
[2] D. Shechtman, I. Blech, D. Gratias, and J. W. Cahn, Metallic Phase with Long-Range Orientational Order and No Translational Symmetry, Phys. Rev. Lett. **53**, 1951 (1984).
[3] N. G. de Bruijn, Algebraic theory of Penrose's non-periodic tilings of the plane. I, Indagationes Mathematicae (Proceedings) **84**, 39 (1981).
[4] N. G. de Bruijn, Algebraic theory of Penrose's non-periodic tilings of the plane. II, Indagationes Mathematicae (Proceedings) **84**, 53 (1981).
[5] P. Kramer and R. Neri, On periodic and non-periodic space fillings of Em obtained by projection, Acta Crystallogr. Sect. A **40**, 580 (1984).
[6] A. I. Goldman and R. F. Kelton, Quasicrystals and crystalline approximants, Rev. Mod. Phys. **65**, 213 (1993).
[7] W. Steurer, Quasicrystals: What do we know? what do we want to know? what can we know? Acta Crystallogr. Sect. A **74**, 1 (2018).
[8] C. Gross and I. Bloch, Quantum simulations with ultracold atoms in optical lattices, Science **357**, 995 (2017).
[9] K. Viebahn, M. Sbroscia, E. Carter, J.-C. Yu, and U. Schneider, Matter-Wave Diffraction from a Quasicrystalline Optical Lattice, Phys. Rev. Lett. **122**, 110404 (2019).
[10] L. Sanchez-Palencia and L. Santos, Bose-Einstein condensates in optical quasicrystal lattices, Phys. Rev. A **72**, 053607 (2005).
[11] J. E. Lye, L. Fallani, C. Fort, V. Guarrera, M. Modugno, D. S. Wiersma, and M. Inguscio, Effect of interactions on the localization of a Bose-Einstein condensate in a quasiperiodic lattice, Phys. Rev. A **75**, 061603(R) (2007).
[12] A. Cetoli and E. Lundh, Loss of coherence and superfluid depletion in an optical quasicrystal, J. Phys. B **46**, 085302 (2013).
[13] A. Jagannathan and M. Duneau, An eightfold optical quasicrystal with cold atoms, Europhys. Lett. **104**, 66003 (2013).
[14] P. Bordia, H. Lüschen, S. Scherg, S. Gopalakrishnan, M. Knap, U. Schneider, and I. Bloch, Probing Slow Relaxation and Many-Body Localization in Two-Dimensional Quasiperiodic Systems, Phys. Rev. X **7**, 041047 (2017).
[15] S. Spurrier and N. R. Cooper, Semiclassical dynamics, berry curvature, and spiral holonomy in optical quasicrystals, Phys. Rev. A **97**, 043603 (2018).
[16] J. Hou, H. Hu, K. Sun, and C. Zhang, Superfluid-Quasicrystal in a Bose-Einstein Condensate, Phys. Rev. Lett. **120**, 060407 (2018).
[17] J. Goldstein, Emergence as a construct: History and issues, Emergence **1**, 49 (1999).
[18] P. A. Corning, The re-emergence of "emergence": A venerable concept in search of a theory, Complexity **7**, 18 (2002).
[19] S. Gopalakrishnan, I. Martin, and E. A. Demler, Quantum Quasicrystals of Spin-Orbit-Coupled Dipolar Bosons, Phys. Rev. Lett. **111**, 185304 (2013).
[20] J. Hou, H. Hu, K. Sun, and C. Zhang, Superfluid-Quasicrystal in a Bose-Einstein Condensate, Phys. Rev. Lett. **120**, 060407 (2018).

[21] R. Lifshitz and D. M. Petrich, Theoretical Model for Faraday Waves with Multiple-Frequency Forcing, Phys. Rev. Lett. **79**, 1261 (1997).
[22] A. R. Denton and H. Löwen, Stability of Colloidal Quasicrystals, Phys. Rev. Lett. **81**, 469 (1998).
[23] M. Engel and H.-R. Trebin, Self-Assembly of Monatomic Complex Crystals and Quasicrystals with a Double-Well Interaction Potential, Phys. Rev. Lett. **98**, 225505 (2007).
[24] K. Barkan, H. Diamant, and R. Lifshitz, Stability of quasicrystals composed of soft isotropic particles, Phys. Rev. B **83**, 172201 (2011).
[25] J. Rottler, M. Greenwood, and B. Ziebarth, Morphology of monolayer films on quasicrystalline surfaces from the phase field crystal model, J. Phys. Condens. Matter **24**, 135002 (2012).
[26] A. J. Archer, A. M. Rucklidge, and E. Knobloch, Quasicrystalline Order and a Crystal-Liquid State in a Soft-Core Fluid, Phys. Rev. Lett. **111**, 165501 (2013).
[27] K. Barkan, M. Engel, and R. Lifshitz, Controlled Self-Assembly of Periodic and Aperiodic Cluster Crystals, Phys. Rev. Lett. **113**, 098304 (2014).
[28] T. Dotera, T. Oshiro, and P. Ziherl, Mosaic two-lengthscale quasicrystals, Nature (London) **506**, 208 (2014).
[29] X. Zeng, G. Ungar, Y. Liu, V. Percec, A. E. Dulcey, and J. K. Hobbs, Supramolecular dendritic liquid quasicrystals, Nature (London) **428**, 157 (2004).
[30] K. Hayashida, T. Dotera, A. Takano, and Y. Matsushita, Polymeric Quasicrystal: Mesoscopic Quasicrystalline Tiling in *abc* Star Polymers, Phys. Rev. Lett. **98**, 195502 (2007).
[31] S. Fischer, A. Exner, K. Zielske, J. Perlich, S. Deloudi, W. Steurer, P. Lindner, and S. Förster, Colloidal quasicrystals with 12-fold and 18-fold diffraction symmetry, Proc. Natl. Acad. Sci. U.S.A. **108**, 1810 (2011).
[32] C. Xiao, N. Fujita, K. Miyasaka, Y. Sakamoto, and O. Terasaki, Dodecagonal tiling in mesoporous silica, Nature (London) **487**, 349 (2012).
[33] J. Zhang and F. S. Bates, Dodecagonal quasicrystalline morphology in a poly(styrene-b-isoprene-b-styrene-b-ethylene oxide) tetrablock terpolymer, J. Am. Chem. Soc. **134**, 7636 (2012).
[34] H. Ritsch, P. Domokos, F. Brennecke, and T. Esslinger, Cold atoms in cavity-generated dynamical optical potentials, Rev. Mod. Phys. **85**, 553 (2013).
[35] P. Domokos and H. Ritsch, Collective Cooling and Self-Organization of Atoms in a Cavity, Phys. Rev. Lett. **89**, 253003 (2002).
[36] K. Baumann, C. Guerlin, F. Brennecke, and T. Esslinger, Dicke quantum phase transition with a superfluid gas in an optical cavity, Nature (London) **464**, 1301 (2010).
[37] D. Schmidt, H. Tomczyk, S. Slama, and C. Zimmermann, Dynamical Instability of a Bose-Einstein Condensate in an Optical Ring Resonator, Phys. Rev. Lett. **112**, 115302 (2014).
[38] J. Klinder, H. Keßler, M. R. Bakhtiari, M. Thorwart, and A. Hemmerich, Observation of a Superradiant Mott Insulator in the Dicke-Hubbard Model, Phys. Rev. Lett. **115**, 230403 (2015).
[39] J. Léonard, A. Morales, P. Zupancic, T. Esslinger, and T. Donner, Supersolid formation in a quantum gas breaking a continuous translational symmetry, Nature (London) **543**, 87 (2017).
[40] J. Léonard, A. Morales, P. Zupancic, T. Donner, and T. Esslinger, Monitoring and manipulating higgs and goldstone modes in a supersolid quantum gas, Science **358**, 1415 (2017).
[41] A. Morales, P. Zupancic, J. Léonard, T. Esslinger, and T. Donner, Coupling two order parameters in a quantum gas, Nat. Mater. **17**, 686 (2018).
[42] M. Landini, N. Dogra, K. Kroeger, L. Hruby, T. Donner, and T. Esslinger, Formation of a Spin Texture in a Quantum Gas Coupled to a Cavity, Phys. Rev. Lett. **120**, 223602 (2018).
[43] R. M. Kroeze, Y. Guo, V. D. Vaidya, J. Keeling, and B. L. Lev, Spinor Self-Ordering of a Quantum Gas in a Cavity, Phys. Rev. Lett. **121**, 163601 (2018).
[44] Y. Guo, R. M. Kroeze, V. D. Vaidya, J. Keeling, and B. L. Lev, Sign-Changing Photon-Mediated Atom Interactions in Multimode Cavity Quantum Electrodynamics, Phys. Rev. Lett. **122**, 193601 (2019).
[45] V. D. Vaidya, Y. Guo, R. M. Kroeze, K. E. Ballantine, A. J. Kollár, J. Keeling, and B. L. Lev, Tunable-Range, Photon-Mediated Atomic Interactions in Multimode Cavity QED, Phys. Rev. X **8**, 011002 (2018).
[46] D. S. Naik, G. Kuyumjyan, D. Pandey, P. Bouyer, and A. Bertoldi, Bose–Einstein condensate array in a malleable optical trap formed in a traveling wave cavity, Quantum Sci. Technol. **3**, 045009 (2018).
[47] S. C. Schuster, P. Wolf, D. Schmidt, S. Slama, and C. Zimmermann, Pinning Transition of Bose-Einstein Condensates in Optical Ring Resonators, Phys. Rev. Lett. **121**, 223601 (2018).
[48] J. G. Cosme, C. Georges, A. Hemmerich, and L. Mathey, Dynamical Control of Order in a Cavity-Bec System, Phys. Rev. Lett. **121**, 153001 (2018).
[49] C. Georges, J. G. Cosme, L. Mathey, and A. Hemmerich, Light-Induced Coherence in an Atom-Cavity System, Phys. Rev. Lett. **121**, 220405 (2018).
[50] R. M. Kroeze, Y. Guo, and B. L. Lev, Dynamical Spin-Orbit Coupling of a Quantum Gas, Phys. Rev. Lett. **123**, 160404 (2019).
[51] H. Habibian, A. Winter, S. Paganelli, H. Rieger, and G. Morigi, Bose-Glass Phases of Ultracold Atoms Due to Cavity Backaction, Phys. Rev. Lett. **110**, 075304 (2013).
[52] K. E. Ballantine, B. L. Lev, and J. Keeling, Meissner-like Effect for a Synthetic Gauge Field in Multimode Cavity QED, Phys. Rev. Lett. **118**, 045302 (2017).
[53] A. U. J. Lode and C. Bruder, Fragmented Superradiance of a Bose-Einstein Condensate in an Optical Cavity, Phys. Rev. Lett. **118**, 013603 (2017).
[54] F. Mivehvar, S. Ostermann, F. Piazza, and H. Ritsch, Driven-Dissipative Supersolid in a Ring Cavity, Phys. Rev. Lett. **120**, 123601 (2018).
[55] F. Mivehvar, H. Ritsch, and F. Piazza, Cavity-Quantum-Electrodynamical Toolbox for Quantum Magnetism, Phys. Rev. Lett. **122**, 113603 (2019).
[56] E. I. Rodríguez Chiacchio and A. Nunnenkamp, Dissipation-Induced Instabilities of a Spinor Bose-Einstein Condensate Inside an Optical Cavity, Phys. Rev. Lett. **122**, 193605 (2019).

[57] A. B. Zamolodchikov, Integrals of motion and S-matrix of the (scaled) $T = \mathrm{Tc}$ Ising-model with magnetic-field, Int. J. Mod. Phys. A **04**, 4235 (1989).
[58] R. Coldea, D. A. Tennant, E. M. Wheeler, E. Wawrzynska, D. Prabhakaran, M. Telling, K. Habicht, P. Smeibidl, and K. Kiefer, Quantum criticality in an Ising chain: Experimental evidence for emergent e8 symmetry, Science **327**, 177 (2010).
[59] P. Chen, Z.-L. Xue, I. P. McCulloch, M.-C. Chung, C.-C. Huang, and S.-K. Yip, Quantum Critical Spin-2 Chain with Emergent Su(3) Symmetry, Phys. Rev. Lett. **114**, 145301 (2015).
[60] E. Sagi and Z. Nussinov, Emergent quasicrystals in strongly correlated systems, Phys. Rev. B **94**, 035131 (2016).
[61] J. Lang, F. Piazza, and W. Zwerger, Collective excitations and supersolid behavior of bosonic atoms inside two crossed optical cavities, New J. Phys. **19**, 123027 (2017).
[62] Z. Wu, Y. Chen, and H. Zhai, Emergent symmetry at superradiance transition of a bose condensate in two crossed beam cavities, Science bulletin **63**, 542 (2018).
[63] E. I. Rodríguez Chiacchio and A. Nunnenkamp, Emergence of continuous rotational symmetries in ultracold atoms coupled to optical cavities, Phys. Rev. A **98**, 023617 (2018).
[64] Y. Guo, V. D. Vaidya, R. M. Kroeze, R. A. Lunney, B. L. Lev, and J. Keeling, Emergent and broken symmetries of atomic self-organization arising from Gouy phase shifts in multimode cavity QED, Phys. Rev. A **99**, 053818 (2019).
[65] G. Baskaran and P. W. Anderson, Gauge theory of high-temperature superconductors and strongly correlated fermi systems, Phys. Rev. B **37**, 580 (1988).
[66] T. Senthil, A. Vishwanath, L. Balents, S. Sachdev, and M. P. A. Fisher, Deconfined quantum critical points, Science **303**, 1490 (2004).
[67] G. 't Hooft, A. Rajantie, C. Contaldi, P. Dauncey, and H. Stoica, Emergent quantum mechanics and emergent symmetries, AIP Conf. Proc. **957**, 154 (2007).
[68] C. Barceló, R. Carballo-Rubio, F. Di Filippo, and L. J. Garay, From physical symmetries to emergent gauge symmetries, J. High Energy Phys. 10 (2016) 084.
[69] E. Witten, Symmetry and emergence, Nat. Phys. **14**, 116 (2018).
[70] See Supplemental Material at http://link.aps.org/supplemental/10.1103/PhysRevLett.123.210604 for the details of the derivation of the effective optical potential, symmetry considerations, finite-size effects, orders of the quantum phase transitions, and some typical atomic density distributions.
[71] F. Piazza, P. Strack, and W. Zwerger, Bose–Einstein condensation versus Dicke–Hepp–Lieb transition in an optical cavity, Ann. Phys. (Amsterdam) **339**, 135 (2013).
[72] F. Piazza and P. Strack, Quantum kinetics of ultracold fermions coupled to an optical resonator, Phys. Rev. A **90**, 043823 (2014).
[73] One can use instead an azimuthally symmetric harmonic trap in an experiment. The discrete $\mathbf{Z}_2$ symmetries discussed in the text are then absent in the system and the center of the emergent quasicrystal potential is fixed externally at the center of the trap.
[74] D. J. Thouless, Electrons in disordered systems and the theory of localization, Phys. Rep. **13**, 93 (1974).
[75] G. Roux, T. Barthel, I. P. McCulloch, C. Kollath, U. Schollwöck, and T. Giamarchi, Quasiperiodic Bose-Hubbard model and localization in one-dimensional cold atomic gases, Phys. Rev. A **78**, 023628 (2008).
[76] The somewhat rugged boundaries are partially due to finite-size effects as discussed in Supplemental Material [70]. Furthermore, parameter grids in the phase diagrams were somewhat coarse as the numerical simulations were quite time consuming due to the lack of periodic boundary conditions.
[77] G. Roati, C. D'Errico, L. Fallani, M. Fattori, C. Fort, M. Zaccanti, G. Modugno, M. Modugno, and M. Inguscio, Anderson localization of a non-interacting Bose–Einstein condensate, Nature (London) **453**, 895 (2008).
[78] J. Billy, V. Josse, Z. Zuo, A. Bernard, B. Hambrecht, P. Lugan, D. Clément, L. Sanchez-Palencia, P. Bouyer, and A. Aspect, Direct observation of Anderson localization of matter waves in a controlled disorder, Nature (London) **453**, 891 (2008).
[79] I. B. Mekhov, C. Maschler, and H. Ritsch, Probing quantum phases of ultracold atoms in optical lattices by transmission spectra in cavity quantum electrodynamics, Nat. Phys. **3**, 319 (2007).
[80] I. B. Mekhov, C. Maschler, and H. Ritsch, Cavity-Enhanced Light Scattering in Optical Lattices to Probe Atomic Quantum Statistics, Phys. Rev. Lett. **98**, 100402 (2007).
[81] K. Gietka, F. Mivehvar, and H. Ritsch, Supersolid-Based Gravimeter in a Ring Cavity, Phys. Rev. Lett. **122**, 190801 (2019).
[82] V. Torggler, P. Aumann, H. Ritsch, and W. Lechner, A quantum n-queens solver, Quantum **3**, 149 (2019).
[83] S. Gopalakrishnan, Y. E. Shchadilova, and E. Demler, Intertwined and vestigial order with ultracold atoms in multiple cavity modes, Phys. Rev. A **96**, 063828 (2017).